A Wind and Rain Backscatter Model Derived From AMSR and SeaWinds Data

Seth N. Nielsen and David G. Long, *Fellow, IEEE*

***Abstract*—The SeaWinds scatterometer was originally designed to measure wind vectors over the ocean by exploiting the relationship between wind-induced surface roughening and the normalized radar backscatter cross section. Rain can degrade scatterometer wind estimation; however, the simultaneous wind/rain (SWR) algorithm was developed to enable SeaWinds to simultaneously retrieve wind and rain rate data. This algorithm is based on colocating data from the Precipitation Radar on the Tropical Rainfall Measuring Mission and SeaWinds on QuikSCAT. This paper develops a new wind and rain radar backscatter model for SWR using colocated data from the Advanced Microwave Scanning Radiometer (AMSR) and SeaWinds aboard the Advanced Earth Observing Satellite II. This paper accounts for rain height in the model in order to calculate surface rain rate from the integrated rain rate. The performance of SWR using the new wind/rain model is measured by comparison of wind vectors and rain rates to the previous SWR algorithm, AMSR rain rates, and National Center for Environmental Prediction numerical weather prediction winds. The new SWR algorithm produces more accurate rain estimates and improved winds, and detects rain with a low false alarm rate.**

***Index Terms*—Atmospheric measurements, rain, scattering, wind.**

I. Introduction

THE SEAWINDS scatterometer has flown twice: once on the QuikSCAT satellite, launched in 1999, and once on the Advanced Earth Observing Satellite II (ADEOS II), launched in late 2002. Unlike QuikSCAT, which did not carry a radiometer, ADEOS II carried an Advanced Microwave Scanning Radiometer (AMSR). AMSR measurements can be used to flag and/or correct rain contamination in SeaWinds-derived winds. ADEOS-II, which operated for less than a year, provided a large set of colocated scatterometer and radiometer measurements that are ideal for studying the effect of rain on scatterometer measurements on a global scale. This paper exploits this data set to develop a wind and rain backscatter model derived from SeaWinds and AMSR on ADEOS II, incorporates the model into the simultaneous wind/rain (SWR) algorithm, and validates the model and algorithm. The SWR algorithm can be applied to QuikSCAT data to compensate for the lack of coincident radiometer measurements and thus add value to data collected by SeaWinds on QuikSCAT.

Scatterometer-based wind retrieval over the ocean is made possible by the relationship between near-surface winds and the normalized radar backscatter cross section σ^o. This relationship is known as the geophysical model function (GMF) [1], [2]. The wind is retrieved by inverting the GMF through estimating the wind speed and direction that are most likely to have caused the measured σ^o [3].

The SeaWinds scatterometer has been shown to retrieve highly accurate wind vectors for most conditions over the Earth's oceans [4], [5]; however, the performance of the wind retrieval is degraded when rain is present [6], [7]. Many studies have been conducted on the effects of rain on radar backscatter particularly as it applies to scatterometer-based wind retrieval, e.g., [7]–[10]. The effect rain has on the observed backscatter is complicated and depends on the rain rate and wind speed among other factors. In general, at Ku-band, rain tends to increase the backscatter, causing the retrieved wind speed to appear greater than the true wind speed [11]. Rain-corrupted wind tends to point orthogonal to the satellite track or cross swath regardless of the true wind direction [12]. Thus, uncompensated rain contamination introduces biases in the scatterometer-retrieved winds. As previously noted, while radiometer measurements can be used to identify rain-contamination in scatterometer-retrieved winds for ADEOS-II, QuikSCAT requires a method for dealing with rain using only scatterometer measurements.

Algorithms have been developed to flag scatterometer data for rain by thresholding a modified objective function of the σ^o observations [13], [14] or by using a multidimensional histogram involving several rain-sensitive parameters [12]. A rain rate and rain flag product has also been derived from the scatterometer noise-only measurements [15], [16]. Some studies have developed wind and rain backscatter models in order to improve wind retrieval by separating the rain-induced backscatter from wind-induced backscatter. Stiles and Yueh [17] developed a backscatter model by determining an affine relationship between the measured σ^o and the wind-only σ^o. The slope and intercept of the relationship were related to Special Sensor Microwave/Imager integrated rain rates via linear regression. Hilburn *et al.* [18] derived a wind and rain backscatter model using colocated data from AMSR and SeaWinds data on ADEOS II. Their synergistic model combines active and passive remote sensor data to correct scatterometer wind estimates in the presence of rain.

Draper and Long [7], [19] incorporated a wind and rain backscatter model into an SWR retrieval algorithm, which is

Manuscript received August 20, 2007; revised May 5, 2008 and August 7, 2008. First published December 12, 2008; current version published May 22, 2009.

The authors are with the Microwave Earth Remote Sensing Laboratory, Electrical and Computer Engineering Department, Brigham Young University, Provo, UT 84602 USA (e-mail: long@ee.byu.edu).

Color versions of one or more of the figures in this paper are available online at http://ieeexplore.ieee.org.

Digital Object Identifier 10.1109/TGRS.2008.2007492

capable of extracting both wind and rain data from scatterometer measurements; however, the performance of the algorithm degrades outside the tropical region (between 35° N and 35° S latitude). The original model that Draper and Long [7] developed for the SWR algorithm used colocated data from the SeaWinds scatterometer on QuikSCAT and the Precipitation Radar on the Tropical Rainfall Measuring Mission (TRMM PR), which only covered the tropical region. Thus, since rain parameters vary with latitude, the accuracy of the model decreases outside of this region.

In this paper, a new wind/rain backscatter model is developed that is calibrated to AMSR data. We use ADEOS-II SeaWinds and AMSR data to develop the model and evaluate its performance with SWR. This paper is motivated by our desire to apply the technique to SeaWinds on QuikSCAT, which has no radiometer to aid in rain detection and retrieval. By comparing the SWR performance of ADEOS-II SeaWinds and AMSR, we can understand the SWR performance expected for QuikSCAT, thus extending the capability of the QuikSCAT mission. The new wind/rain model is based on the same phenomenological backscatter model used by Draper and Long to represent the effects of rain on SeaWinds backscatter; however, rain height is included, and the rain data for this paper is provided by the AMSR radiometer as opposed to the TRMM PR. Climatology maps of rain height are derived in this paper for use in the SWR algorithm. The wind vectors used to derive the model come from the National Center for Environmental Prediction (NCEP) numerical weather prediction wind fields. Rain rate and rain parameters are derived from the colocated measurements of SeaWinds and AMSR aboard ADEOS II. The new model is used with the SWR algorithm to estimate winds and rain over the SeaWinds mission. These are validated by comparison to AMSR-derived rain rates and NCEP winds.

Section II of this paper describes the instruments and the data sets used in this paper. In Section III, we develop the new wind and rain backscatter model by extracting the model parameters from the data sets and relating the rain-induced parameters to rain rate. Rain height climatology tables are derived and compared in Section IV. The updated SWR algorithm is used to process SeaWinds on ADEOS II data, which is compared to the original SWR-processed SeaWinds data, AMSR rain rates, and NCEP wind vectors. The results of these comparisons are presented in Section V.

II. Instruments and Data

The ADEOS II satellite carried both SeaWinds and AMSR. The measurements of the two sensors are colocated in space except for the outermost portion of AMSR's swath. There is no more than 2.5 min between colocated measurements [18].

SeaWinds is a Ku-band pencil-beam scatterometer operating at a frequency of 13.4 GHz [20]. It uses two circularly scanning beams at fixed incidence angles with different polarizations. The outer beam is vertically polarized (v-pol) with an incidence angle of 54° and the inner beam is horizontally polarized (h-pol) with an incidence angle of 46°. With a swath width of 1800 km, SeaWinds covers about 90% of the Earth's surface daily. SeaWinds measures the normalized radar backscatter cross section, σ^o, at multiple azimuth angles. In conventional wind processing, maximum likelihood estimation is used to invert the GMF to retrieve wind vector ambiguities, which are the most probable wind vectors for the given σ^o observations within a 25 km × 25 km square, or wind vector cell (WVC). The resulting wind vector ambiguities then undergo a dealiasing process to select the ambiguities that most closely match the true wind field.

AMSR is an eight-frequency radiometer with both v-pol and h-pol measurements for all frequencies except two. The antenna scans a semicircular pattern in front of the spacecraft at a fixed incidence angle of 55°, giving AMSR a slightly wider swath (1900 km) than SeaWinds. AMSR measures brightness temperatures at various frequencies that are processed to obtain various geophysical parameters like sea surface temperature (SST), atmospheric liquid, and rain. The AMSR level 2A overlay (L2Ao) files, provided by the Jet Propulsion Laboratory (JPL), report parameters such as rain rate and SST on a grid designed to overlay the SeaWinds L2B product [21]. The AMSR overlay data are divided into 12.5 km × 12.5 km squares, or WVC quadrants (WVCQs), with four quadrants inside each WVC. AMSR data are also used to calculate the rain attenuation at SeaWinds' operating frequency. This rain attenuation measurement is contained in the SeaWinds L2A data structure for each σ^o measurement.

This paper also makes use of NCEP model winds, which are numerically predicted winds calculated every 6 h with a very coarse resolution $(2.5^\circ \times 2.5^\circ)$. Because of this coarse resolution, small-scale wind features and rain effects are not included in the prediction. NCEP thus provides an estimate of the mean rain-free wind. These predicted winds are interpolated in space and time to each SeaWinds WVC and are included in the L2B files; however, the NCEP wind speeds are biased high when compared to the winds retrieved by SeaWinds [22]. The method for correcting this bias is presented in Section III-A. The next section describes the derivation of the wind/rain model function.

III. Wind and Rain Backscatter Model

Rain has three major effects on radar backscatter: raindrops roughen the ocean's surface, which tends to augment the surface backscatter; raindrops falling in the atmosphere attenuate the radar signal as it travels to and from the ocean's surface; and atmospheric rain also backscatters the signal. We model these rain-induced effects with a simple phenomenological model [19]

$$\sigma_{\mathrm{m}} = (\sigma_{\mathrm{w}} + \sigma_{\mathrm{sr}})\alpha_{\mathrm{r}} + \sigma_{\mathrm{r}} \tag{1}$$

where σ_{m} is the backscatter measured by SeaWinds, σ_{w} is the surface backscatter from wind-induced capillary waves, σ_{sr} is the surface backscatter due to raindrop splash products, α_{r} is the two-way atmospheric rain attenuation, and σ_{r} is the volume scattering due to atmospheric rain.

The three rain-effect parameters σ_{sr}, α_{r}, and σ_{r} are functions of the integrated rain rate, which is modeled as the product of

surface rain rate and rain height. The $\sigma_{\rm sr}$ term is a simplified model for the average rain-induced surface perturbation effect and ignores the interaction between wind and rain. Since we are only interested in the bulk effect of surface perturbation due to rain, an additive parameter is deemed sufficient. Because SeaWinds can provide very little information on drop size distribution and vertical profile, the atmospheric rain parameters ($\alpha_{\rm r}$ and $\sigma_{\rm r}$) are not explicitly parameterized in terms of these terms. This is a limitation of the technique. To simplify the backscatter model of (1), we combine the rain effects into a more compact form [7]

$$\sigma_{\rm m} = \sigma_{\rm w}\alpha_{\rm r} + \sigma_{\rm e} \tag{2}$$

where $\sigma_{\rm e} = \sigma_{\rm sr}\alpha_{\rm r} + \sigma_{\rm r}$ is the effective rain backscatter. This model combines three sources of uncertainty into two. The following sections demonstrate the method of calculating the parameters of the model and the relation of the rain parameters to the integrated rain rate.

A. Estimation of Wind-Only Backscatter and Bias Correction

The wind-only backscatter term $\sigma_{\rm w}$ of (2) represents the backscatter due to wind when no rain is present, which corresponds to the conventional wind-only GMF. In order to derive the other model parameters, $\sigma_{\rm w}$ is calculated from the NCEP model winds contained in the SeaWinds L2B product and the standard QuikSCAT GMF, QMOD3 [3]. The NCEP wind vectors are interpolated to the center latitude and longitude of each SeaWinds σ^o measurement by performing a cubic spline interpolation of the orthogonal wind vector components separately. The interpolated vector components are recombined to obtain the speed and direction of the interpolated wind vectors. These are then projected through the GMF in order to estimate the wind-only backscatter at each σ^o location

$$\sigma_{\rm w(NCEP)} = \mathcal{M}\left(u_{\rm (NCEP)}, \chi_{\rm (NCEP)}, \theta, {\rm pol}\right) \tag{3}$$

where $\mathcal{M}$ represents the GMF, $u_{\rm (NCEP)}$ is the interpolated NCEP wind speed, $\chi_{\rm (NCEP)}$ is the relative azimuth angle of the interpolated NCEP wind vector, θ is the incidence angle, and pol is the beam polarization.

$\sigma_{\rm w(NCEP)}$ is a biased estimate of the actual $\sigma_{\rm w}$ because the NCEP winds themselves are biased relative to SeaWinds winds as mentioned previously. Due to the low resolution of NCEP winds, we assume that the bias is spatially correlated. We estimate the bias, ϵ, for each σ^o observation as a weighted average of the difference between $\sigma_{\rm m}$ and $\sigma_{\rm w}$ for all rain-free observations in the same look direction, either fore or aft. We define rain-free observations as those with rain rate less than 0.01 because 0.01 mm/hr is the lowest rain rate that AMSR can detect. The bias error of the jth observation is

$$\epsilon^j = \frac{\sum_i W^{ij}\left(\sigma^i_{m({\rm SW})} - \sigma^i_{\rm w(NCEP)}\right)}{\sum_i W^{ij}} \tag{4}$$

where the index i sums over all rain-free observations of the same look direction as the jth observation, and $\sigma^i_{m({\rm SW})}$ is the backscatter measured by SeaWinds. W^{ij} is the Epanechnikov weighting function for the ith and jth observations, which is calculated by

$$W^{ij} = \begin{cases} 1 - \left(\frac{d(i,j)}{r}\right)^2, & d(i,j) \le r \\ 0, & \text{otherwise} \end{cases} \tag{5}$$

where r is a radius in kilometers around the jth observation and $d(i,j)$ is the distance between the ith and jth observations in km. Nominally, r is 20 km unless there are fewer than two observations within 20 km, in which case the radius is dilated by adding 10 km at a time until at least two observations are found within the radius. $\sigma_{\rm w}$ can now be written as the sum of the backscatter predicted from the NCEP winds and the bias error

$$\sigma_{\rm w} = \sigma_{\rm w(NCEP)} + \epsilon. \tag{6}$$

The mean bias of the training data set is -0.0021 with a standard deviation of 0.0052, which is consistent with the observation that NCEP winds are biased slightly high compared to SeaWinds winds. These values are comparable to a mean of -0.0025 and standard deviation of 0.0064 observed in [7].

B. Calculation of Rain Parameters

Before presenting the calculation of the rain model parameters, we discuss the differences between the viewing geometries of SeaWinds and AMSR that affect the accuracy of the rain model. The v-pol measurement of SeaWinds has an incidence angle of 54°, which is similar to AMSR's 55° incidence angle; however, SeaWinds' h-pol measurements are at an incidence angle of 46°. The AMSR rain attenuation, as contained in the AMSR L2Ao files, is computed empirically for each σ^o observation where the difference in incidence angles is implicitly taken into account [21]. SeaWinds' observations can be fore or aft with respect to the orientation of the spacecraft, whereas AMSR only looks forward. This difference in azimuth observation angle relative to the spacecraft is not addressed in computing the rain attenuation.

Partial beam filling is not explicitly accounted for in estimating the model parameters. Partial beam filling occurs when the horizontal extent of a rain cell is smaller than the width of the radar beam passing through it. Hilburn *et al.* [18] accounts for partial beam filling in their ocean wind correction algorithm by means of an effective temperature depression that is calculated from AMSR brightness temperatures. This approach cannot be used for QuikSCAT. Correcting for partial beam filling from SeaWinds data alone is impractical [7] and is not attempted here.

To derive the rain model function, the two rain model parameters of (2), $\alpha_{\rm r}$ and $\sigma_{\rm e}$, are calculated from AMSR data. The SeaWinds L2A files include an empirical calculation of the attenuation due to atmospheric water. An estimate of

other sources of attenuation (e.g., clouds and water vapor) is subtracted from this attenuation term to yield the attenuation due to rain alone (see [23]). Estimates of the effective rain backscatter can be computed using the estimates of wind-only backscatter and rain attenuation by rearranging the terms in (2)

$$\sigma_{\mathrm{e}} = \sigma_{\mathrm{m}} - \left(\sigma_{\mathrm{w(NCEP)}} + \epsilon\right) \alpha_{\mathrm{r(AMSR)}}. \tag{7}$$

The following section discusses the relationship between these two model parameters and integrated rain rate.

C. Relation of Rain Parameters to Integrated Rain Rate

AMSR rain rate data from the L2Ao files is interpolated to the center latitude and longitude of each SeaWinds σ^o observation in order to observe the effect rain has on backscatter. The rain rate for a given σ^o measurement is set to the value of the nearest neighboring AMSR WVCQ. Nearest neighbor interpolation is done for simplicity, while a more rigorous approach could use a weighted average of nearby cells based on the gain pattern of the antenna.

The rain model parameters of (2) are functions of the integrated rain rate; however, the AMSR L2Ao files report only the surface rain rate and provide no rain height estimate. Using a technique similar to that of [24], SSTs from the AMSR L2Ao files are used to estimate rain heights [21], which in turn are used to compute the integrated rain rate.

We model the relationship of atmospheric rain attenuation and effective rain backscatter to integrated rain rate as quadratic polynomials of integrated rain rate

$$10\log_{10}\left(-\left(\alpha_{\mathrm{r(AMSR)}}\right)_{\mathrm{dB}}\right) \approx f_{\mathrm{a}}(R_{\mathrm{ir}}) = \sum_{n=0}^{2} c_{\mathrm{a}}(n) R_{\mathrm{ir}}^{n} \tag{8}$$

$$(\sigma_{\mathrm{e}})_{\mathrm{dB}} \approx f_{\mathrm{e}}(R_{\mathrm{ir}}) = \sum_{n=0}^{2} c_{\mathrm{e}}(n) R_{\mathrm{ir}}^{n} \tag{9}$$

where R_{ir} is the integrated rain rate in decibels. α_{r} is converted to decibels twice in (8) in order to facilitate fitting the data with a quadratic polynomial, similar to [7].

The training data set used to calculate the model parameters include data from the L2A, L2Ao, and L2B files and is composed of one orbit selected randomly from each day of the ADEOS II mission. In order to avoid sea-ice contamination near the poles, only data between 60° S and 60° N latitude are included. R_{ir} is calculated from the AMSR L2Ao files, the $\alpha_{\mathrm{r(AMSR)}}$ term is taken from the SeaWinds L2A file (note that it is calculated based on AMSR data even though it is found in the SeaWinds data set [21]), and the $\sigma_{\mathrm{w(NCEP)}}$ and ϵ terms are derived from the NCEP winds found in the SeaWinds L2B files. Only the portions of the swath where both h-pol and v-pol measurements are available are used in the data set, so roughly five million colocated data points are used to calculate the h-pol parameter coefficients and three million are used to calculate the v-pol coefficients. We solve for the quadratic polynomial coefficients c_{a} and c_{r} by casting (8) and (9) into matrix form and using least-squares. The model coefficients are recorded in Table I for both h-pol and v-pol observations. These attenuation and effective rain backscatter models are valid for integrated rain rates between 0.01 and 100 km · mm/h. The full wind and rain backscatter model is

TABLE I
COEFFICIENTS OF THE QUADRATIC FITS TO THE PARAMETERS α_{r} AND σ_{e} IN (8) AND (9), RESPECTIVELY

	$c_a(0)$	$c_a(1)$	$c_a(2)$
h-pol	-9.2879	1.0379	-0.0151
v-pol	-9.0998	1.1747	-0.022
	$c_e(0)$	$c_e(1)$	$c_e(2)$
h-pol	-28.6900	1.0817	-0.0197
v-pol	-27.3168	0.7168	-0.0106

$$\begin{aligned}\sigma_{\mathrm{m}}(s,d,R_{\mathrm{ir}}) &= \sigma_{\mathrm{w}}(s,d)\alpha_{\mathrm{r}}(R_{\mathrm{ir}}) + \sigma_{\mathrm{e}}(R_{\mathrm{ir}}) \\ &= \sigma_{\mathrm{w}}(s,d)10^{-10^{f_{\mathrm{a}}(R_{\mathrm{ir}})/10}/10} + 10^{f_{\mathrm{e}}(R_{\mathrm{ir}})/10}\end{aligned} \tag{10}$$

where s and d are the wind speed and direction.

Figs. 1 and 2 compare the rain model parameters to those of [7]. For the remainder of this paper, we refer to the model in [7] as the Draper–Long SWR (DL-SWR) model while our model is referred to as the AMSR-SeaWinds SWR (AS-SWR) model. The range of values are comparable for both parameters and both polarizations; however, the behavior of the two models is slightly different. For the scales shown in the plot of Fig. 1, the DL-SWR attenuation model appears nearly linear, whereas the AS-SWR attenuation model appears more parabolic. The attenuation values for the AS-SWR model are lower than those of the DL-SWR model for the lowest and the highest integrated rain rates. The fact that the attenuation values of the AS-SWR model appear to level off at higher rain rates may be due to the effect of partial beam filling for the empirically calculated attenuation values. Convective storms tend to have high rain rates and have small physical scales [21], [25], [26]; therefore, they only partially fill the SeaWinds' footprint. This suggests that on average the partial beam-filling effect is included in the empirical calculation of the attenuation. For increasing integrated rain rates, σ_{e} is larger for the h-pol beam than it is for the v-pol beam, as has been noted in previous investigations [7], [17].

IV. RAIN HEIGHT

The SWR algorithm estimates an irregularly weighted spatially averaged *integrated* rain rate for each WVC [19]. AMSR estimates rain rate, so in order to compare the two methods of rain retrieval, an estimate of the rain height is necessary to convert integrated rain rate to surface rain rate. SeaWinds has only very coarse range resolution and cannot measure rain height from the time of flight of the radar return like the TRMM PR. Thus, for this paper, rain height is provided by a simple climatology. The following sections examine the statistics of rain height and the different methods of incorporating rain height into the SWR algorithm.

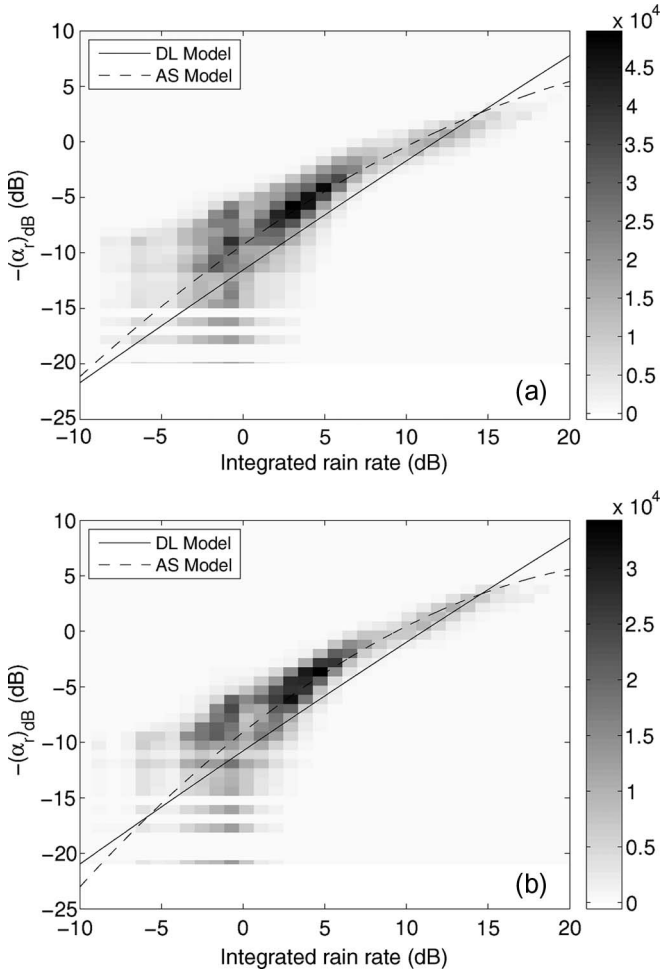

Fig. 1. Scatter density plot of atmospheric rain attenuation versus integrated rain rate for the (a) h-pol and (b) v-pol beams. The model fit to the data for the DL-SWR and AS-SWR models are shown. There are approximately 4 million points in each plot.

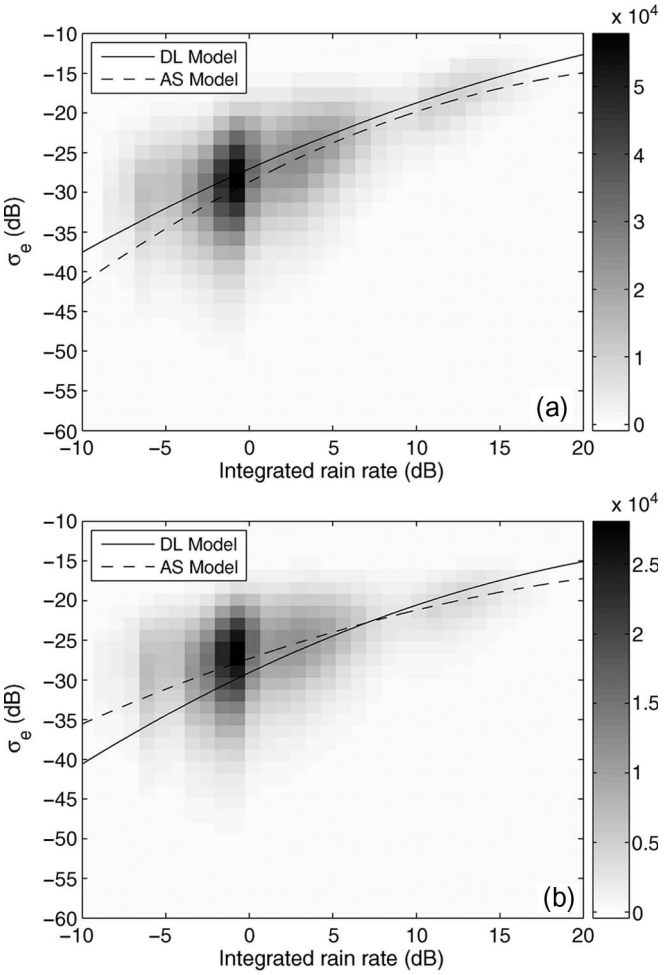

Fig. 2. Scatter density plot of effective rain backscatter versus integrated rain rate for the (a) h-pol and (b) v-pol beams. The model fit to the data for the DL-SWR and AS-SWR models are shown. There are approximately 4 million points in each plot.

A. Rain Height Climatology

Previous studies [27], [28] have shown that rain height is a function of latitude, longitude, and season. The AMSR-derived rain heights in the current study also demonstrate these dependences. For example, Fig. 3 shows a plot of rain height versus latitude. The bands that occur at discrete rain heights are due to the quantization of the AMSR data used to calculate the rain heights. The nonparametric fit to the data represents the mean rain height of each latitude bin. We note that the mean rain height is low at high latitudes and reaches a peak near the equator. This figure demonstrates a strong connection between rain height and latitude; however, there is a great deal of spread in the rain heights for a given latitude bin, particularly in the northern hemisphere, which has a higher average rain height compared to the southern hemisphere. Rain height variability contributes to the variability in the AS-SWR-derived rain rate estimates.

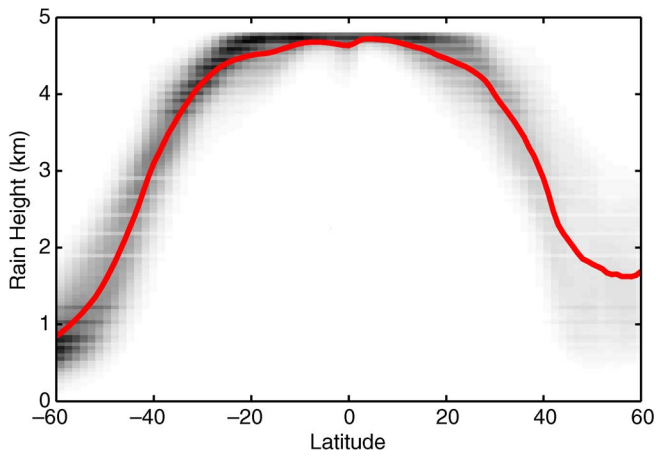

Fig. 3. Scatter density of rain height versus latitude and a nonparametric approximation of the mean rain height for May 2003. Rain heights are derived from AMSR SST data.

B. Rain Height Tables

Mean rain height tables based on different combinations of latitude, longitude, and Julian day are created and compared based on the R^2 goodness of fit, which provides a measure of how much the fit accounts for the variance of the rain height. A summary of these statistics for the different tables is presented in Table II. Latitude is the largest factor for determining rain

TABLE II
VARIANCE OF THE RAIN HEIGHT DIFFERENCES FOR THE VARIOUS MEAN RAIN HEIGHT TABLES

Table No.	Index Parameters	Variance	R^2
h	-	2.08	0%
1	Lat.	0.23	88.9%
2	Lat. Day	0.17	91.8%
3	Lat. Lon.	0.16	92.1%
4	Lat. Lon. Day	0.06	97.3%

height, accounting for nearly 90% of the variance in rain height by itself. The most complete model includes all three index parameters and accounts for 97% of the variance. The combination of latitude and longitude marginally outperforms the combination of latitude and day, both accounting for roughly 92% of the variance. Including seasonal (day) dependence improves the accounting to 97% of the variance. Simulation suggests that including seasonal dependence in the SWR algorithm reduces the rain error variance by less than 0.01 mm/h.

Since ADEOS II failed before a full year's worth of data could be acquired, the rain height statistics are limited to the months between April and October. Thus, we cannot form a rain height table that is indexed by day or season for use outside of these months. We therefore do not include seasonal dependence for the remainder of this paper and use a height table based only on latitude and longitude. We note that the temporal distribution of rain height data limits the accuracy of the latitude and longitude rain height maps because the mean rain height is biased toward the values of the summer months. Future work to improve the rain height table should use a longer data set of rain heights to generate annual climatological rain height maps.

For wind retrieval, the original DL-SWR algorithm is modified to use the AS-SWR wind/rain model and the latitude- and longitude-based table of mean rain heights discussed in this section. The modified retrieval is termed the AS-SWR algorithm and is validated in the next section.

V. VALIDATION RESULTS

To validate the performance of the AS-SWR algorithm, data from the entire SeaWinds on ADEOS II mission are processed using the AS-SWR algorithm. Results and statistics presented in this section are for the entire mission unless otherwise stated. Rain rates from the AS-SWR algorithm are compared to AMSR rain rates and wind vectors are compared to NCEP winds only in locations where AMSR, DL-SWR, or AS-SWR detects rain. In order to convert DL-SWR integrated rain rates to surface rain rates, the DL-SWR integrated rain rates are divided by the rain heights provided by the rain height table used by AS-SWR.

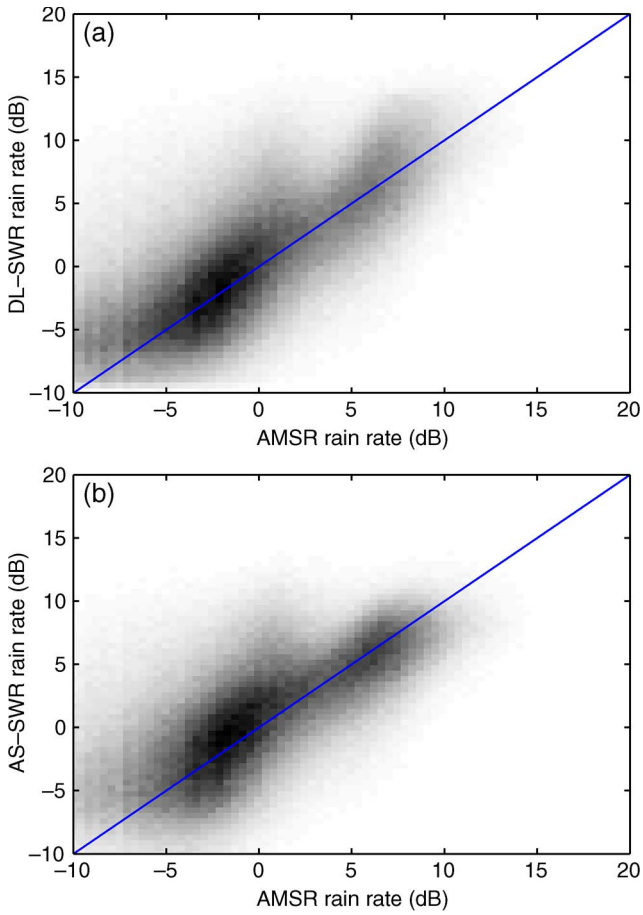

Fig. 4. Scatter density plots from May 2003 of: (a) AMSR rain rates versus DL-SWR rain rates and (b) AMSR rain rates versus AS-SWR rain rates. Rain rates are expressed in decibels. The equality line is shown for comparison.

A. Rain Rate Comparison

This section compares AS-SWR and DL-SWR rain retrieval to that of AMSR rain estimates. Fig. 4(b) shows a scatter density plot of AMSR rain rates versus bias-corrected AS-SWR rain rates for one month. We note that raw AS-SWR retrieved rain rates are biased high compared to AMSR. This bias is corrected by adjusting the rain model parameter coefficients of Table I according to the technique presented in [29]. For comparison, Fig. 4(a) shows a similar plot for bias-corrected DL-SWR rain rates. In both cases, the rain rate thresholds discussed in [30] are used to discard rain rates that are deemed spurious.

Comparing Fig. 4(a) and (b), the variance in the AS-SWR rain rates is noticeably improved compared to DL-SWR. For the data shown in Fig. 4, the correlation coefficient of DL-SWR with AMSR rain rates is 0.64, while the correlation coefficient of AS-SWR with AMSR rain rates is 0.61. For the entire mission, the mean residual bias of DL-SWR relative to AMSR rain rates is −0.86 mm/h and the mean residual bias of AS-SWR relative to AMSR rain rates is −0.55 mm/h. Overall, the DL-SWR rain rates have a slightly higher correlation, but the AS-SWR rain rates have less residual bias and less variance at higher rain rates. As discussed later, the AS-SWR rain rates are more accurate over a wider latitude range than DL-SWR.

TABLE III
SUMMARY OF BACKSCATTER REGIMES

Regime Number	Rain Fraction $F = \sigma_e/\sigma_m$	Description
0	$F < 0.25$	Wind dominates backscatter
1	$0.25 \leq F \leq 0.75$	Wind and rain backscatter are comparable
2	$0.75 < F$	Rain dominates backscatter

TABLE IV
CORRELATION COEFFICIENTS AND MEAN AND RMS DIFFERENCES FOR DL-SWR AND THE AS-SWR RAIN RATES COMPARED TO AMSR RAIN RATES. CORRELATION COEFFICIENTS ARE COMPUTED FOR THE DECIBEL RAIN RATES WHILE THE MEAN AND RMS DIFFERENCES ARE COMPUTED FOR LINEAR SCALE RAIN RATES. A NEGATIVE DIFFERENCE INDICATES THE SWR RAIN RATES ARE LARGER THAN THE AMSR RAIN RATES ON AVERAGE

Regime	Correlation coefficient		Mean difference (mm/hr)		RMS difference (mm/hr)	
	DL-SWR	AS-SWR	DL-SWR	AS-SWR	DL-SWR	AS-SWR
all	0.64	0.61	-0.86	-0.55	3.89	2.96
0	0.27	0.20	-0.1127	-1.08	1.953	3.613
1	0.57	0.54	-0.6098	-0.4465	3.564	3.165
2	0.81	0.74	-1.694	-0.6443	4.979	2.573

To demonstrate the SWR algorithm's ability to separate wind and rain effects on backscatter, each WVC is classified by backscatter regime from the backscatter measurements. The regime is determined by the estimated rain fraction defined as the ratio of effective rain backscatter to the total measured backscatter, $F = \sigma_{\rm e}/\sigma_{\rm m}$. Table III contains a summary of these backscatter regimes. The rain rate data sets are binned by backscatter regime and the correlation coefficient and the mean and rms differences (in linear scale, not dB scale) are calculated for all regimes. These statistics are summarized in Table IV. The data in regime 2 have the highest correlation coefficients because rain dominates the backscatter and the rain estimates have a higher quality than the other regimes. The data in regime 0 has the lowest correlation coefficients because wind dominates the backscatter and degrades the quality of rain estimation. Rain estimation in this regime can be expected to be unreliable. Overall, AS-SWR has lower mean and rms differences relative to AMSR rain rates than DL-SWR. When the data are binned by regime, the DL-SWR mean and rms error is the smallest in regime 1 and largest in regime 2. Although the variation with regime is smaller for AS-SWR, AS-SWR has an opposite trend, with the smallest errors at the highest regime number. This is consistent with expectations since the rain retrieval should be less accurate in wind-dominated regime 0 and more accurate in rain-dominated regime 2. This topic is further discussed in later paragraphs.

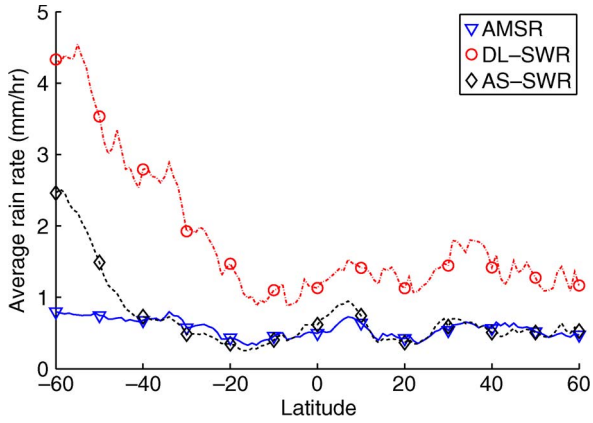

Fig. 5. Average rain rates binned by latitude for AMSR, DL-SWR, and AS-SWR for June 2003. We note that DL-SWR consistently overestimates the average rain rate, while AS-SWR only does so at high latitudes in the southern hemisphere.

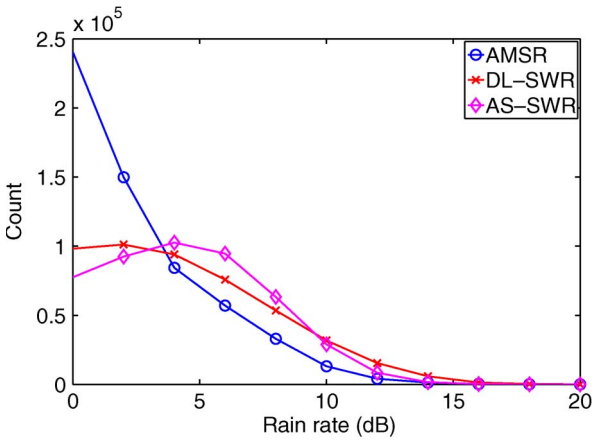

Fig. 6. Histograms of rain rates for AMSR, DL-SWR, and AS-SWR for July 2003. Data includes only WVCs where the backscatter regimes of DL- and AS-SWR are the same.

Fig. 5 shows the average rain rate versus latitude for the month of June 2003. AS-SWR average rain rates resemble the AMSR rain rates more than DL-SWR rain rates except in the southernmost latitudes (between 40° and 60° S latitude) where AS-SWR rain rates become larger than AMSR's. DL-SWR average rain rates are larger than AMSR's and they become increasingly larger at 20° S latitude and below. This suggests that AS-SWR has improved rain retrieval performance over a broader range of latitudes. This is not surprising since DL-SWR was developed by comparison with only tropical rains via TRMM-PR, whereas AS-SWR uses global AMSR measurements.

We check the consistency of DL- and AS-SWR rain rate estimates with AMSR rain rates by comparing the distributions of rain rate estimates. Fig. 6 shows histograms of AMSR, DL-SWR, and AS-SWR rain rates from WVCs where both SWR algorithms detect the same rain backscatter regime. AMSR's histogram is nearly exponential and highly concentrated at low rain rates, whereas DL- and AS-SWR are more concentrated at higher rain rates. We note that scatterometer

backscatter measurements have proportionally more noise than do AMSR brightness temperature measurements. This is reflected in the histograms of the rain estimates, which reflect the convolution of the exponential true (AMSR) rain rate distribution and the Gaussian distribution of the backscatter measurement error. The backscatter error "spreads" the distribution. Since the rain rate cannot be negative, spreading has the effect of decreasing the number of low rain observations and increasing the number of high rain measurements. This effect is further enhanced by the nonorthogonal nature of backscatter signature of rain and wind, which can confuse rain effects and wind speed at certain wind directions [19].

Fig. 7 shows rain rate histograms for the same data binned by backscatter regime. We note that in regime 0, poor rain retrievals are expected since the backscatter is dominated by wind, i.e., there is limited sensitivity of backscatter to rain. In regime 2, the observed backscatter is dominated by rain and should result in the best rain accuracy (but poor wind accuracy). We note that in regime 2, rain accuracy can be improved by using a rain-only retrieval algorithm [31], although this algorithm is not applied here.

As in Fig. 6, the SWR histograms reflect the convolution of the true exponential rain histogram with the normal distribution of the noise in the backscatter measurements. As anticipated, in regime 0 where rain accuracy is expected to be poor, the rain is underestimated at low rain rates, although it becomes more accurate at higher rain rates. The large deviation of the SWR histograms from the AMSR histogram in regimes 1 and 2 is due, in part, to errors in estimating the correct regime, as well as measurement noise. SWR histograms for regimes 1 and 2 erroneously include a higher proportion of low rain rates from regime 0 due to regime classification errors which alter the observed distribution. Nevertheless, for both regimes 1 and 2, AS-SWR is more accurate than DL-SWR at lower rain rates although both DL-SWR and AS-SWR overestimate the occurrence of low rain rates.

Clearly, SWR rain rates are inferior to AMSR-derived rain rates, which would be preferred for rain rate retrieval during the ADEOS-II mission. However, since the QuikSCAT platform does not carry a radiometer, these results are useful for understanding the utility of the AS-SWR rain rates during the QuikSCAT mission. We note that SWR also provides improved wind estimates, particularly in regime 1.

Overall, AS-SWR has improved rain retrieval capabilities compared to DL-SWR. Despite DL-SWR's somewhat higher correlation with AMSR rain rates, AS-SWR rain rates are generally more accurate and precise. The accuracy of AS-SWR rain estimates improves as the rain contributes more significantly to the backscatter in regimes 1 and 2. The monthly average rain rates of AS-SWR and AMSR are comparable for a broad range of latitudes, whereas DL-SWR average rain rates are larger than AMSR rain rates across all latitudes.

As a secondary comparison we consider AS-SWR-derived rain rates and "SRAD" rain estimates derived from SeaWinds noise-only measurements [15], [16]. We note that the scatterometer noise-only measurements are interleaved with its signal power measurements so that the SRAD observations are naturally collocated in time and space with the SWR measurements. However, in SRAD processing, spatial averaging is used to reduce the noise and variability. This has the effect of lowering the effective resolution of the SRAD rain estimates compared to the SWR measurements, which has a side effect of increasing relative variability with AS-SWR. We note that the SRAD measurements have a large ΔT compared to AMSR measurements.

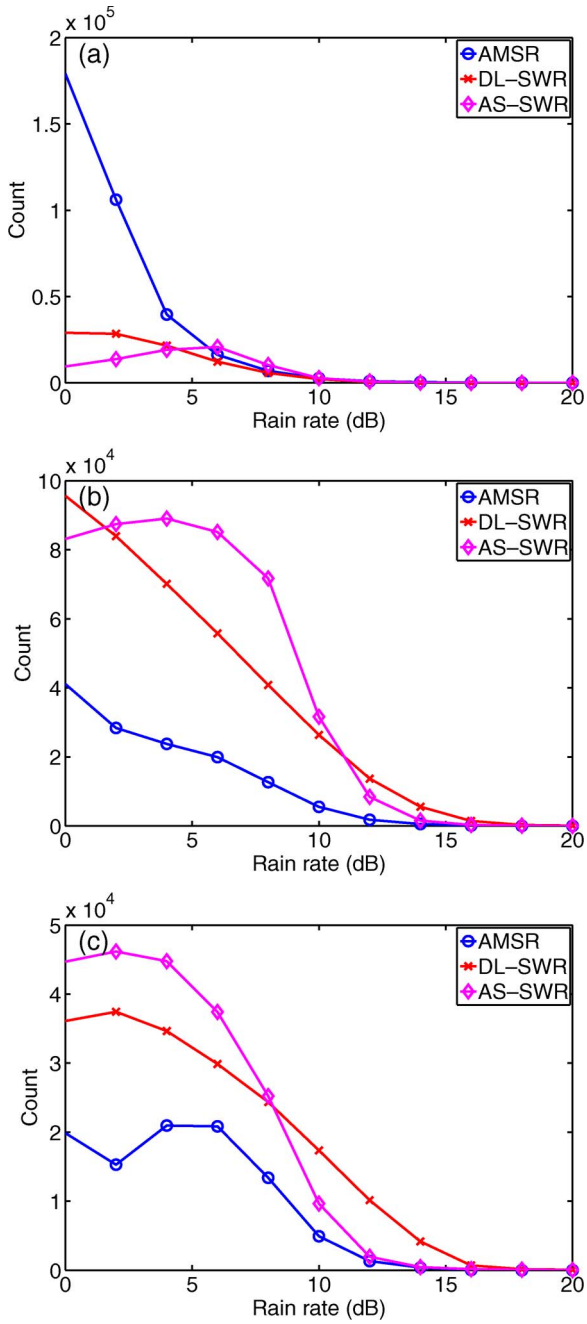

Fig. 7. Histograms of AMSR, DL-SWR, and AS-SWR rain rates for (a) regime 0, (b) regime 1, and (c) regime 2 for July 2003.

A comparison of AS-SWR and SRAD rain rates is shown in Fig. 8. The SRAD measurements are biased approximately 6 mm/h lower than the AS-SWR measurements. While a general correlation trend is observed (correlation coefficient $\sim$0.4), there is significant variability. The high scatter arises from the high levels of noise in the two data sets and limits the utility of

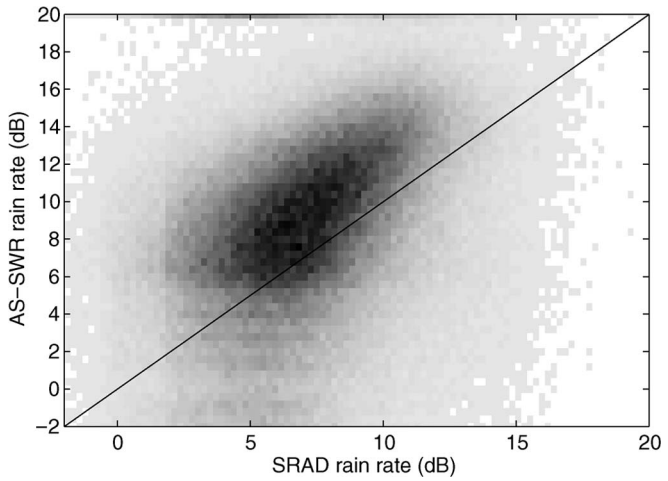

Fig. 8. Scatter density plot of AS-SWR versus SRAD rain rates for May 2003. Data includes all WVCs with nonzero rain rate estimates.

the comparison. While the scatterometer noise-only measurements are used in signal power estimation in computing the backscatter measurement, the backscatter measurement error is dominated by Rayleigh fading and thermal noise during the signal power measurement. Thus, the measurement errors (noise) in the SRAD and AS-SWR rain estimates are effectively independent. The high noise level is similar for all regimes, but as expected, a variation in correlation with regime is observed: The correlation is the lowest (0.35) for backscatter regime 0 where wind dominates (and thus AS-SWR is the least accurate), and the largest (0.41) for rain-dominated regime 2 where AS-SWR is the most accurate.

B. Rain Flag Comparison

The comparisons made in the previous section are primarily in areas where AMSR and AS-SWR or AMSR and DL-SWR both detect nonzero rain. This section compares the ability of the DL- and AS-SWR algorithms to detect rain in the same regions as AMSR. The SWR algorithms' rain rates can be used to flag wind-only retrievals for rain contamination. We compare the rain flagging ability of AS-SWR to the rain impact flag in the SeaWinds L2B file and to DL-SWR rain rates. The two metrics of flagging ability are false alarm rate and missed detection rate. A false alarm occurs when the WVC is flagged for rain but the AMSR rain rate is zero. A missed detection occurs when the WVC is not flagged and AMSR shows a nonzero rain rate. For this comparison, rain is detected by a particular algorithm if the rain rate is greater than 0.01 mm/h. Increasing the threshold decreases both the false alarm rate and the missed detection rate.

Table V contains a summary of the false alarm and missed detection rates for the three rain flags under consideration. The L2B flag, which for ADEOS-II includes AMSR data, is asserted when rain has an appreciable impact on the accuracy of wind retrieval [12]. While the L2B rain impact flag has the lowest false alarm rate and the highest missed detection rate compared to the other algorithms, its accuracy is reduced on QuikSCAT. AS-SWR has a smaller false alarm rate than DL-SWR but has a higher missed detection rate. The difference in both cases

TABLE V
COMPARISON OF THREE RAIN FLAGS: DL-SWR RAIN RATE, AS-SWR RAIN RATE, AND THE SEAWINDS L2B RAIN IMPACT FLAG

Rain Flag	False alarm rate	Missed detection rate
DL-SWR	6.8%	41.9%
AS-SWR	5.7%	42.9%
L2B rain impact flag	0.2%	47%

TABLE VI
COMPARISON OF WIND RETRIEVAL PERFORMANCE OF THE L2B, DL-SWR, AND AS-SWR ALGORITHMS AGAINST NCEP WINDS. NCEP WIND SPEEDS ARE MULTIPLIED BY 0.83

	Speed (m/s)			Direction (°)		
	Corr. coeff.	Mean diff.	RMS diff.	Corr. coeff.	Mean diff.	RMS diff.
L2B	0.78	-1.29	2.81	0.95	0.98	32
DL SWR	0.85	-0.84	2.21	0.96	0.69	29.1
AS SWR	0.83	-0.64	2.26	0.96	1.03	29.4

is about 1%, indicating that the performance of both SWR algorithms in detecting rain is comparable. We note that SWR rain flag accuracy is independent of the availability of AMSR data. We note that the rain rate thresholds of [30] can be updated and calibrated with the L2B rain impact flag to lower the false alarm rate by increasing the missed detection rate.

C. Wind Vector Comparison

This section compares the performance of AS-SWR wind retrieval to that of DL-SWR using NCEP winds as a comparison data set. Although NCEP winds have coarse resolution both temporally and spatially, they are not affected by rain. The original SeaWinds wind vectors ("L2B winds") are also included in this analysis to serve as a point of reference for wind retrieval without consideration of rain. The correlation coefficient, mean difference, and rms difference of speed and direction with respect to NCEP wind vectors are computed for all three wind vector data sets. To account for the bias between NCEP and SeaWinds wind vectors, NCEP winds are multiplied by 0.83 [7], [19]. Table VI summarizes the statistical comparison. Overall, the performance of both SWR algorithms is comparable. Both SWR algorithms are an improvement over L2B processing.

To demonstrate AS-SWR's ability to correct rain contamination of wind retrieval, Fig. 9 shows normalized histograms of wind speed for AS-SWR, L2B, and NCEP winds. All three sets compare well under no-rain conditions. In wind-dominated regime 0, the scatterometer wind distributions are comparable, with just a slight shift to slightly higher wind speeds. The slight bias is due in part to variability in the rain-induced backscatter

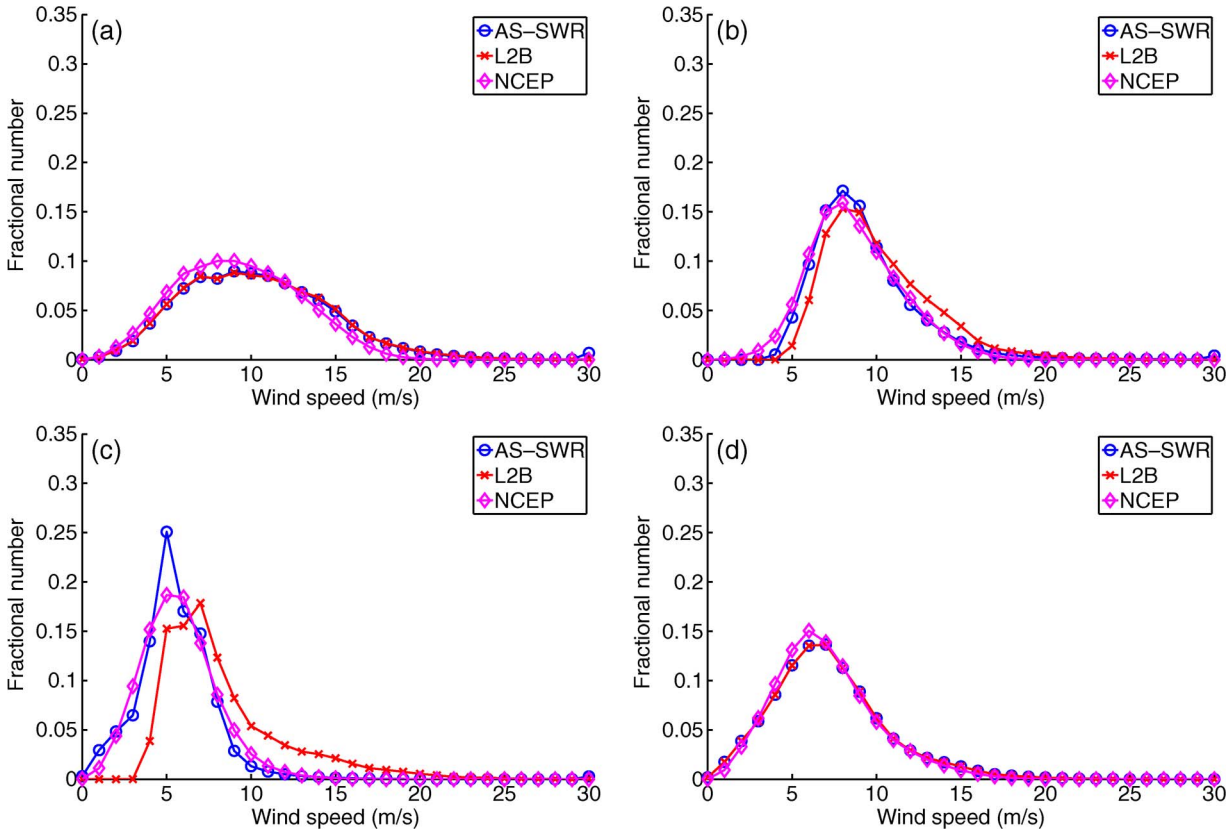

Fig. 9. Normalized histograms of wind speed of AS-SWR, L2B, and NCEP winds for (a) regime 0, (b) regime 1, (c) regime 2, and (d) where no rain is present. Regime 0—wind dominates. Regime 1—wind and rain are comparable. Regime 2—rain dominates. Data are from May 2003.

being converted to positive wind speed error and in part due to errors in regime identification error. Thus, some regime 1 cases are included in the regime 0 histogram. In regime 1, the L2B wind distribution is clearly shifted high, while the AS-SWR distribution matches the NCEP distribution. This pattern is even more pronounced in rain-dominated regime 2.

Fig. 10 shows normalized histograms of wind direction relative to the satellite track for AS-SWR, L2B, and NCEP winds. A direction of 0° corresponds to along-track while 90° and 270° correspond to winds blowing in the cross-track direction. For no-rain conditions, all three data sets match as expected. Similarly, in wind-dominated regime 0 the wind direction histograms match closely. In regimes 1 and 2, NCEP winds exhibit a bias toward cross-track winds that increases with rain. The AS-SWR wind direction histograms generally match the NCEP directions, although some evidence of cross-track bias remains. This occurs because the backscatter signatures of wind and rain are more similar for winds that blow cross-track [19].

D. Results Summary

The AS-SWR and DL-SWR methods both produce more accurate winds than conventional processing. While overall rain performance is generally similar for the two SWR algorithms, AS-SWR rain rates are generally more accurate and precise than those of DL-SWR. AS-SWR has fewer false rain rates than DL-SWR, but it misses more true rain rates. The rain flagging capability of the DL- and AS-SWR algorithms are comparable; however, comparison to the AMSR-derived rain impact flag suggests that the flagging capability can be improved if SWR rain rate thresholds are adjusted. Both SWR algorithms improve the accuracy of wind estimates compared to L2B winds. In comparison to NCEP winds, the AS-SWR algorithm corrects the typical effects of rain contamination by lowering artificially high wind speed estimates and by correcting wind vectors that point cross-track due to rain contamination.

VI. Conclusion

A wind and rain backscatter model derived from AMSR and SeaWinds on ADEOS II has been implemented in the SWR algorithm. A climatological map of the mean rain height derived from AMSR data are used by the SWR algorithm to produce surface rain rate estimates comparable to those of AMSR, although noisier. AS-SWR rain estimates are an improvement compared to DL-SWR rain estimation. They are generally more accurate and precise and have a wider latitude range. AS-SWR also corrects much of the latitude-based errors in rain rate estimates to which DL-SWR is subject. The wind vector correction capability of the algorithm is effective at reducing artificially high wind speeds caused by rain-induced backscatter augmentation. The cross-track wind direction bias caused by rain contamination is significantly reduced. While AMSR-derived rain rates may be preferred to SWR-derived rain rates, we conclude that overall, the SWR algorithm is an effective method of improving the accuracy of SeaWinds

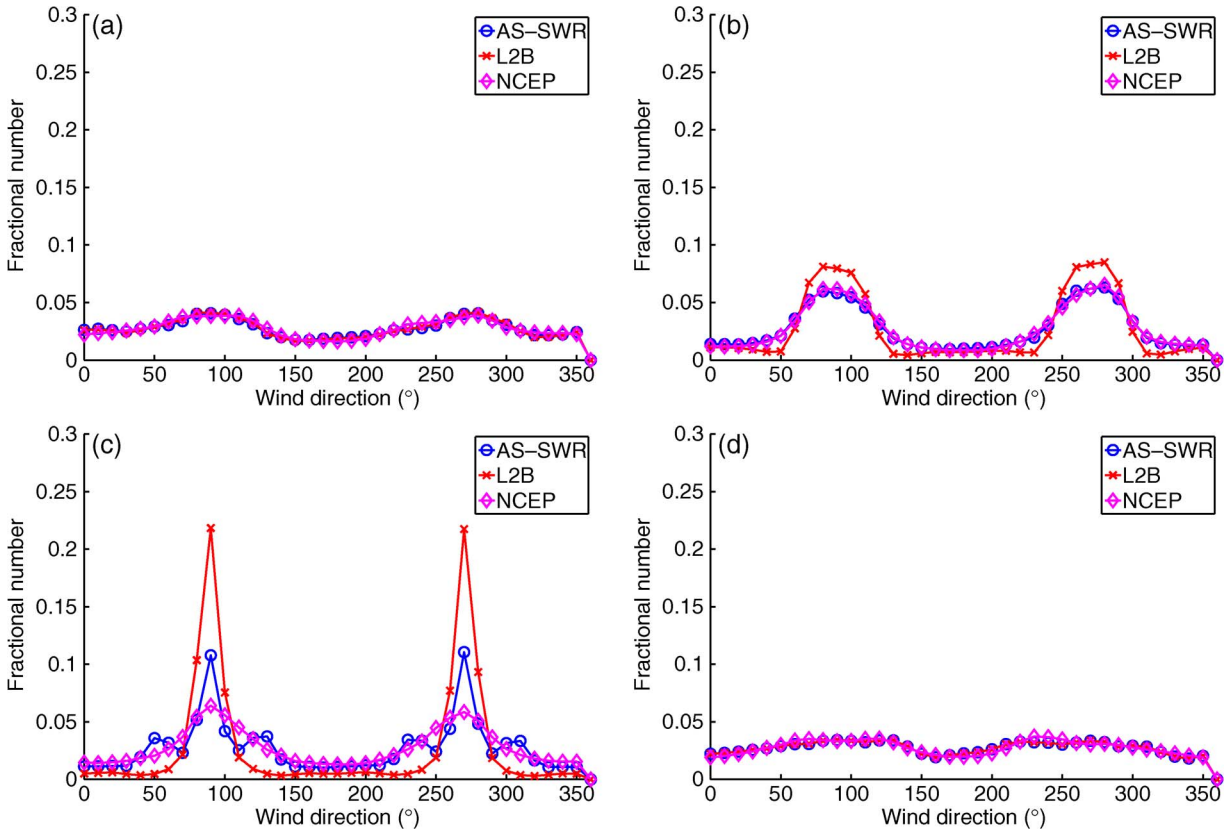

Fig. 10. Normalized histograms of wind direction of AS-SWR, L2B, and NCEP winds (relative to the satellite track) for (a) backscatter regime 0, (b) regime 1, (c) regime 2, and (d) where no rain is present. Regime 0—wind dominates; regime 1—wind and rain are comparable; regime 2—rain dominates. Data are from May 2003.

scatterometer wind retrieval and has the added benefit of retrieving contemporaneous rain rates when radiometer data are not available for QuikSCAT.

Acknowledgment

The authors would like to thank M. Owen for his help with figures. Data was obtained from the JPL PO.DAAC http://podaac.jpl.nasa.gov. The authors would also like to thank the anonymous reviewers for their helpful comments.

References

[1] F. T. Ulaby, R. K. Moore, and A. K. Fung, *Microwave Remote Sensing: Active and Passive*, vol. 1. Norwood, MA: Artech House, 1981.

[2] F. J. Wentz and D. K. Smith, "A model function for the ocean-normalized radar cross section at 14 GHz derived from NSCAT observations," *J. Geophys. Res.*, vol. 104, no. C5, pp. 11 499–11 514, May 1999.

[3] T. Lungu, "QuikSCAT science data product user's manual," Jet Propulsion Lab., Los Angeles, CA, Tech. Rep. D-18053-Rev. A Ver. 3, Sep. 2006. [Online]. Available: ftp://podaac.jpl.nasa.gov/ocean wind/quikscat/L2B/doc/QSUG v3.pdf

[4] P. Queffeulou and A. Bentamy, "Comparison between QuikSCAT and altimeter wind speed measurements," in *Proc. IEEE Int. Geosci. Remote Sens. Symp.*, Jul. 2000, vol. 1, pp. 269–271. DOI: 10.1109/IGARSS.2000.860488.

[5] Z. Jelenak, L. N. Connor, and P. S. Chang, "The accuracy of high resolution winds from QuikSCAT," in *Proc. IEEE Int. Geosci. Remote Sens. Symp.*, vol. 2002, pp. 732–734.

[6] R. N. Hoffman, C. Grassotti, and S. M. Leidner, "SeaWinds validation: Effect of rain as observed by East Coast radars," *J. Atmos. Ocean. Technol.*, vol. 21, no. 9, pp. 1364–1377, Sep. 2004.

[7] D. W. Draper and D. G. Long, "Evaluating the effect of rain on SeaWinds scatterometer measurements," *J. Geophys. Res.*, vol. 109, no. C2, pp. C02 005.1–C02 005.12, 2004.

[8] L. F. Bliven and J. P. Giovanangeli, "Experimental study of microwave scattering from rain- and wind-roughened seas," *Int. J. Remote Sens.*, vol. 14, no. 5, pp. 855–869, 1993.

[9] D. E. Weissman, M. A. Bourassa, and J. Tongue, "Effects of rain rate and wind magnitude on SeaWinds scatterometer wind speed errors," *J. Atmos. Ocean. Technol.*, vol. 19, no. 5, pp. 738–746, May 2002.

[10] R. F. Contreras, W. J. Pland, W. C. Keller, K. Hayes, and J. Nystuen, "Effects of rain on Ku-band backscatter from the ocean," *J. Geophys. Res.*, vol. 108, no. C5, pp. 34.1–34.15, May 2003.

[11] Z. Yang, S. Tang, and J. Wu, "An experimental study of rain effects on fine structures of wind waves," *J. Phys. Oceanogr.*, vol. 27, no. 3, pp. 419–430, Mar. 1997.

[12] J. N. Huddleston and B. W. Stiles, "A multidimensional histogram rain-flagging technique for SeaWinds on QuikSCAT," in *Proc. IEEE Int. Geosci. Remote Sens. Symp.*, Jul. 2000, vol. 3, pp. 1232–1234. DOI: 10.1109/IGARSS.2000.858077.

[13] C. A. Mears, D. Smith, and F. J. Wentz, "Detecting rain with QuikSCAT," in *Proc. IEEE Int. Geosci. Remote Sens. Symp.*, Jul. 2000, vol. 3, pp. 1235–1237. DOI: 10.1109/IGARSS.2000.858078.

[14] M. Portabella and A. Stoffelen, "Rain detection and quality control of SeaWinds," *J. Atmos. Ocean. Technol.*, vol. 18, no. 7, pp. 1171–1183, Jul. 2001.

[15] K. Ahmad, W. Jones, and T. Kasparis, "QuikSCAT radiometer (QRad) rain rates level-2b data product," in *Proc. IEEE Int. Geosci. Remote Sens. Symp.*, Denver, CO, Aug. 28–Sep. 1, 2006, vol. 3.

[16] K. Ahmad, W. Jones, and T. Kasparis, "Oceanic rainfall retrievals using passive and active measurements from SeaWinds," in *Proc. IEEE Int. Geosci. Remote Sens. Symp.*, Barcelona, Spain, Jul. 23–27, 2007, vol. 3.

[17] B. W. Stiles and S. H. Yueh, "Impact of rain on spaceborne Ku-band wind scatterometer data," *IEEE Trans. Geosci. Remote Sens.*, vol. 40, no. 9, pp. 1973–1983, Sep. 2002.

[18] K. A. Hilburn, F. J. Wentz, D. K. Smith, and P. D. Ashcroft, "Correcting active scatterometer data for the effects of rain using passive radiometer data," *J. Appl. Meteorol. Climatol.*, vol. 45, no. 3, pp. 382–398, Mar. 2006.

[19] D. W. Draper and D. G. Long, "Simultaneous wind and rain retrieval using SeaWinds data," *IEEE Trans. Geosci. Remote Sens.*, vol. 42, no. 7, pp. 1411–1423, Jul. 2004.
[20] M. W. Spencer, C. Wu, and D. G. Long, "Tradeoffs in the design of a spaceborne scanning pencil beam scatterometer: Applications to SeaWinds," *IEEE Trans. Geosci. Remote Sens.*, vol. 35, no. 1, pp. 115–126, Jan. 1997.
[21] S. Veleva, personal communication.
[22] *Data release addendum: Data quality overview*, May 2000. QuikSCAT Project Data Release Notes.[Online]. Available: ftp://podaac.jpl.nasa.gov/ocean wind/quikscat/doc/qs-rlsadd.doc
[23] S. Nielsen, "A wind and rain backscatter model derived from AMSR and SeaWinds data," M.S. thesis, Brigham Young Univ., Provo, UT, 2007.
[24] F. J. Wentz and R. W. Spencer, "SSM/I rain retrievals within a unified all-weather ocean algorithm," *J. Atmos. Sci.*, vol. 55, no. 9, pp. 1613–1627, May 1998.
[25] G. Liu and Y. Fu, "The characteristics of tropical precipitation profiles as inferred from satellite radar measurements," *J. Meteorol. Soc. Jpn.*, vol. 79, no. 1, pp. 131–143, Feb. 2001.
[26] E. J. Zipser, *Handbook of Weather, Climate, and Water: Dynamics, Climate, Physical Meteorology, Weather Systems, and Measurements*. Hoboken, NJ: Wiley, 2003.
[27] L. S. Chiu and A. T. C. Chang, "Oceanic rain column height derived from SSM/I," *J. Clim.*, vol. 13, no. 23, pp. 4125–4136, 2000.
[28] M. Thurai, E. Deguchi, K. Okamoto, and E. Salonen, "Rain height variability in the tropics," *Proc. Inst. Elect. Eng.—Microw., Antennas Propag.*, vol. 152, no. 1, pp. 17–23, Feb. 2005.
[29] D. Draper, "Wind scatterometry with improved ambiguity selection and rain modeling," Ph.D. dissertation, Brigham Young Univ., Provo, UT, Dec. 2003.
[30] D. W. Draper and D. G. Long, "Assessing the quality of SeaWinds rain measurements," *IEEE Trans. Geosci. Remote Sens.*, vol. 42, no. 7, pp. 1424–1432, Jul. 2004.
[31] J. R. Allen and D. G. Long, "An analysis of SeaWinds-based rain retrieval in severe weather events," *IEEE Trans. Geosci. Remote Sens.*, vol. 43, no. 12, pp. 2870–2878, Dec. 2005.

Seth N. Nielsen received the M.S. degree in electrical engineering from Brigham Young University (BYU), Provo, UT, in 2007.

He researched scatterometer wind and rain retrieval algorithms with the Microwave Earth Remote Sensing Laboratory, BYU. He is currently an Electrical Engineer with the RF Guidance Engineering Branch, Naval Air Warfare Center Weapons Division, China Lake, CA.

David G. Long (S'80–SM'98–F'07) received the Ph.D. degree in electrical engineering from the University of Southern California, Los Angeles, in 1989.

From 1983 to 1990, he was with NASA's Jet Propulsion Laboratory, where he developed advanced radar remote-sensing systems. While with JPL, he was the Project Engineer on the NASA Scatterometer project which flew from 1996 to 1997. He also managed the Scanning Scatterometer project, the precursor to SeaWinds which was launched, in 1999 and 2002. He is currently a Professor with the Electrical and Computer Engineering Department, Brigham Young University, Provo, UT, where he teaches upper division and graduate courses in communications, microwave remote sensing, radar, and signal processing and is the Director of the BYU Center for Remote Sensing. He is the Principle Investigator on several NASA-sponsored research projects in remote sensing. He has numerous publications in signal processing and radar scatterometry. His research interests include microwave remote sensing, radar theory, space-based sensing, estimation theory, signal processing, and mesoscale atmospheric dynamics. He has over 280 publications.

Dr. Long has received the NASA Certificate of Recognition several times. He is an Associate Editor for IEEE GEOSCIENCE AND REMOTE SENSING LETTERS.